3D PET: Optimization of the Direct Fourier Method of image reconstruction

Fynn Tseng[1]
[1]Department of Bioengineering, University of Washington

1 Abstract

In order to obtain an estimation for oblique 3D PET data, proper interpolation windows must be designed between the data and image spectra. Such a window must be finite in the time-domain (i.e., the sinc interpolator, while ideal, is not a practical candidate) and have coefficients that maximize the signal-to-noise ratio after filtering. It is shown in this novel algorithm that the parameters of the Modified Kaiser-Bessel function (MKB) can be optimized to afford good image quality without the need to zero-pad or oversample. This optimization was carried out for both the forward projection and reconstruction processes. It was found that the parameter values, and robustness to the extent of zero padding, were different for the two steps.

2 Introduction and Background

There is a great thrust to optimize 3D PET because it is a modality with extremely high spatial sensitivity; volumes of activity that are close together can be distinguished. There is a compromise, however, with the sensitivity to randoms and scatters (since Lines of Response may occur between any pair of detectors), which must be attenuated using other algorithms. Detector design, then, is an important aspect of 3D PET optimization (Bailey et al., 1996).

In 2D PET, the resultant image is simply the 2D IDFT of the DFT of the back-projection (modulated by a rho filter) of all projections of the 2D DFT of the data. In order to apply this sort of reconstruction to 3D PET, a more complex filter must be used on the DFT of the back-projection. This is because an infinite number of projections cannot be obtained with the oblique data (the rho filter approximates an infinite number of projection angles). Thus, the reconstruction of images from 3D Positron Emission Tomography (PET) is complicated by the finite geometry of the detector system. If the radiated angle (of photons) is sufficiently large, oblique annihilation events usually miss the detector, and thus are not counted in the gamma (pulse height) spectrum.

The estimation of missing data points from 3D projections is, hence, an integral part of the reconstruction process. Many different algorithms have been developed to implement this estimation. Some classes will be reviewed and discussed herein. The first sort of strategy comprises iterative-based approaches, in which the estimation step is implicit and recursive. One salient example of this form of estimation is the Expectation – Maximization (EM) algorithm, in which the expected likelihood of each event (across the projection space) is maximized. For PET (Rajan et al., 1994), it is assumed that the maximum likelihood function depends on a parameter of a Poisson process (i.e., the number or photons that are emitted from a volume). In the Order Subsets Expectation Maximization (OSEM) algorithm, EM is applied to segments of data (Hudson and Larkin, 1994). The Fourier Rebinning (FORE) algorithm is rather unique because it reduced a 3D data space into 2D sinograms (Kinahan et al, 2000).

The other strategies, one of which is optimized in this paper, are known as Fourier-based reconstructions (FRP). The utility of FRP is contingent on the parameters (which determine the time and frequency behaviors) of an interpolating function that is used to both forward-project

the image spectrum back into an estimate data spectrum, and in the reconstruction process. The FRP algorithms are amenable to the Fast Fourier Transform (FFT), which can reduce the number of complex multiplications by a factor of 2^n, where n is the zero-padded length of the signal. This becomes important in instances where real-time (or approximately real-time) volumetric rendering is an assay for the time-course of the radionuclide.

3 Theory of Direct Fourier Methods

From the truncated oblique data, obtained by 3D PET, there exists at least one axial plane (i.e., in the plane of the scintillators) in which the 2D Fourier transform of the projection (along a defined angle) is equivalent to a line though the 3D Fourier transform of the image. This is a direct consequence of the Fourier Slice Theorem (alternatively known as the Projection Slice Theorem). To show that this is true, consider the projection of an arbitrary cross-sectional area of a volume in $\Re^n$, $f(x_i, x_j)$. The slice though the Fourier transform is:

$$\Im\langle f\rangle(m_p,0,....,0)=\int_{-\infty}^{\infty}\overset{(n-1)}{\cdots}\int_{-\infty}^{\infty} f(x_i,x_j)e^{-2\pi j\sum_{i=1}^{n-1}x_1m_1}\prod_{k=1}^{n-1}dx_k\,dx_n=\int_{-\infty}^{\infty}\overset{(n-1)}{\cdots}\int_{-\infty}^{\infty} f(x,y)e^{-2\pi jx_{p1}m_p}\prod_{k=1}^{n-1}dx_k\,dx_n$$

$$=\int_{-\infty}^{\infty}\overset{(n-1)}{\cdots}\left(\int_{-\infty}^{\infty} f(x,y)dx_n\right)e^{-2\pi jx_{p1}m_p}\prod_{k=1}^{n-1}dx_k=\int_{-\infty}^{\infty}\overset{(n-1)}{\cdots} p(f,x)e^{-2\pi jxm}\prod_{k=1}^{n-1}dx_k$$

where $p(f,x_p)$ is the projection of f along x_p. This method can be used to acquire lines through the data spectrum, since a 1D projection can be obtained with each complete 2D data set. Thus, the reconstruction of 3D data from 2D data is highly amenable to this method during the reprojection stage. In the present algorithm, the PET data is usually rendered in polar coordinates, and the analogous formulation for the projection along subspace θ is as follows (after Matej and Kazantsev, 2006):

$$p(r,\theta)=\int_{\Re^1} x\left(u+\vec{t}\theta\right)d\vec{t} \tag{1}$$

Thus, the Slice Theorem can be rewritten from (1) to yield

$$\Im^{(n-1)}\langle p(r,\theta)\rangle=\Im^{(n)}\langle f(x_0...,x_n)\rangle \tag{2}$$

In Filtered Back-Projection (FBP), the original image, f, is obtained by projecting each 1-D projection upon the appropriate line of response (in this case, designated by the subspace $\vec{t}\theta$. In the ideal 2D FBP, a ramp filter is applied before the IFFT. This in not possible in 3D PET since the projections are truncated in one dimension. Instead, a optimal window, $w(r,\theta)$ must be designed (after Kinahan, 1999) such that

$$f(x,y)=\int_0^{\pi}\int_{-\infty}^{\infty}\Im\langle w(r,\theta)\rangle\Im\langle p(r,\theta)\rangle dw d\theta \tag{3}$$

The optimization of this window is described below, and involves the minimization of error that is incurred during the forward projection and reconstruction. The errors are calculated as the deviations from the ideal sinc interpolation.

4 Optimization Algorithm

The algorithm scheme can be described by six operations on the raw PET data.

1. Quantization and 2D Fourier transformation of initial data (real measurements including actual events, scatters, and randoms).
2. Pre-interpolative weighting to correct for the non-homogeneity in the data spectrum (polar coordinates) relative to the fixed-size interpolation kernel (Kaiser-Bessel).
3. *Interpolation* with the optimized MKB kernel from the data spectrum to the Cartesian image spectrum. This is the novel aspect of the algorithm.
4. Post-interpolative weighting and filtering in the image spectrum domain (to remove effects arising from the non-ideal kernel).
5. 3D inverse Fourier transform to the image domain.
6. Pointwise multiplication of the image by w^{-1}.
7. Reprojection of the initial image by performing the preceding operations in reverse order, using different optimized parameters.
8. Reconstruction of the final image by performing the preceding steps in forward order.

The MKB window has the analytic form:

$$k(\omega) = J(\alpha, m)^{-1}\left[\sqrt{1-(\omega/a)}\right]^{m} \cdot J\left(\alpha\sqrt{1-(\omega/a)}, m\right) \tag{4}$$

Here, $J(\lambda, m)$ is the modified Bessel function (Lewitt, 1990) of order m, on parameter λ. The explicit formulation (after Abramowitz and Stegun, 1972) is

$$J(\alpha, m, \lambda) = i^{-m}\, 2\pi^{-1} \int_{0}^{2\pi} \cos(\alpha\omega + \lambda \sin\omega) d\omega \tag{5}$$

In other words, the characteristics of the MKB window are controlled by three parameters. These are the order m, radius a, and 'governing constant' α, which controls the shape of the main lobe and side-lobes in the frequency domain. These parameters are optimized for the reprojection and reconstruction phases of the algorithm.

The pre-interpolation weights are determined by the iteration (after Matej and Lewitt, 2001), and are necessary because the density of signals in the data spectrum is not constant. A ramp filter, as discussed above, is insufficient since the exact variation of the density is generally not hyperbolically related to r. The iteration is:

$$\kappa\{i+1,(r,\theta)\} = \kappa\{i,(r,\theta)\}\left[\kappa\{i,(r,\theta)\} * k(\omega)\right]^{-1} \; ; \; \kappa\{0,(r,\theta)\} = s(r,\theta)\left[s(r,\theta) * k(\omega)\right]^{-1} \tag{6}$$

The sampling function (similar to the delta function), $s(r,\theta) = 1 \; \forall (r,\theta) \subset P$, simply defines the region to begin the iteration. Here, r and θ are in the frequency-domain. As i becomes large, (6)

yields a final distribution of κ over the data spectrum (i.e., each point is weighted by a different value, determined by the interpolation kernel used). The authors did not carry the iteration out on all values of the data spectrum. The other κ values were obtained by iterating over a subset of P, and subsequently interpolating.

Post-interpolation weights are generally negligible if κ is determined. However, since the number of iterations is finite, there will still be some residual error after interpolation. In theory, the interpolation and weighting procedures are commutative (switching the order gives the same result). The weight function can also be determined analytically, since $\kappa(r,\theta) = s(r,\theta)/\Im\langle k(\omega)\rangle = s(r,\theta)/\lambda(\omega)$. Since the kernel is symmetric in the frequency domain, this ought to be identical to the original $\Im\langle k(\omega)\rangle$. It is not clear why the iterative solution is used, instead of the analytic one.

Thus, the entire algorithm can be expressed by the following mapping of data between the various domains:

$$f(x,y,z) = \Im^{-1,(3)}\left\langle\left\langle\int_{\Re^1}\left(\left\langle\Im^{-1,(3)}\left\langle\Im^{(2)}\left\langle p(r,\theta)\right\rangle\cdot\kappa\left(\bar{r},\bar{\theta}\right)\cdot\Im\langle k(\omega)\rangle\right\rangle\right\rangle + \tau\theta\right)d\tau\right\rangle\cdot\kappa\left(\bar{r},\bar{\theta}\right)\cdot k(\omega)\right\rangle \qquad (7)$$

We have disregarded the post-interpolation weighting or filtering. The image is reconstructed in polar spherical coordinates (since the image has three dimensions). The coordinates in the (x,y,z) system are then found by a standard transformation. The integration is simply the projection step into a coordinate system with an infinite range of angles.

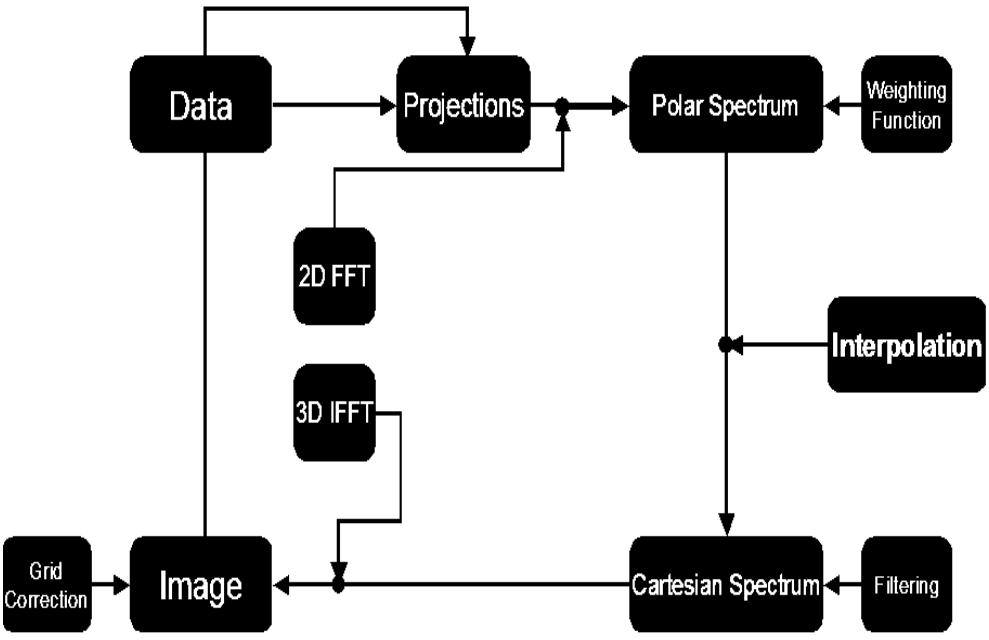

The Fourier Reprojection Algorithm (Recapitulated from above) The zero-padded truncated data is projected at selected angles. The projections are then converted to a polar spectrum through a 2D FFT. A weighting function is applied to this spectrum to homogenize the density data (since the Kernel is finite). This weighted spectrum is then interpolated into Cartesian coordinates by the MKB kernel. Post-interpolative weighting and filtering may be applied (though it is often not necessary, since the first projection provides fairly good estimates. The resulting spectrum is converted into an image through the 3D IFFT. This image is reprojected, and the algorithm is carried again. (Adapted from Matej and Kazantsev, 2006).

5 Demonstration and Proof of Concept

Parameter optimization is carried out by comparing the direct Fourier algorithms (above) with an ideal projection (in the forward projection phase), and for real data (during reconstruction). The normalized mean error is minimized as a function of α for parameters $a = 2.5$, $m = 0$, and z (length of zero-padding). The results are shown in FIGURE 1. As we expect, the windows in the time-domain are rather isomorphic to the common Chebyshev and normal Kaiser filters. The frequency responses look rather different for the forward-projection and reconstruction phases, however. The former is characterized by a sharper transition zone, but less attenuation.

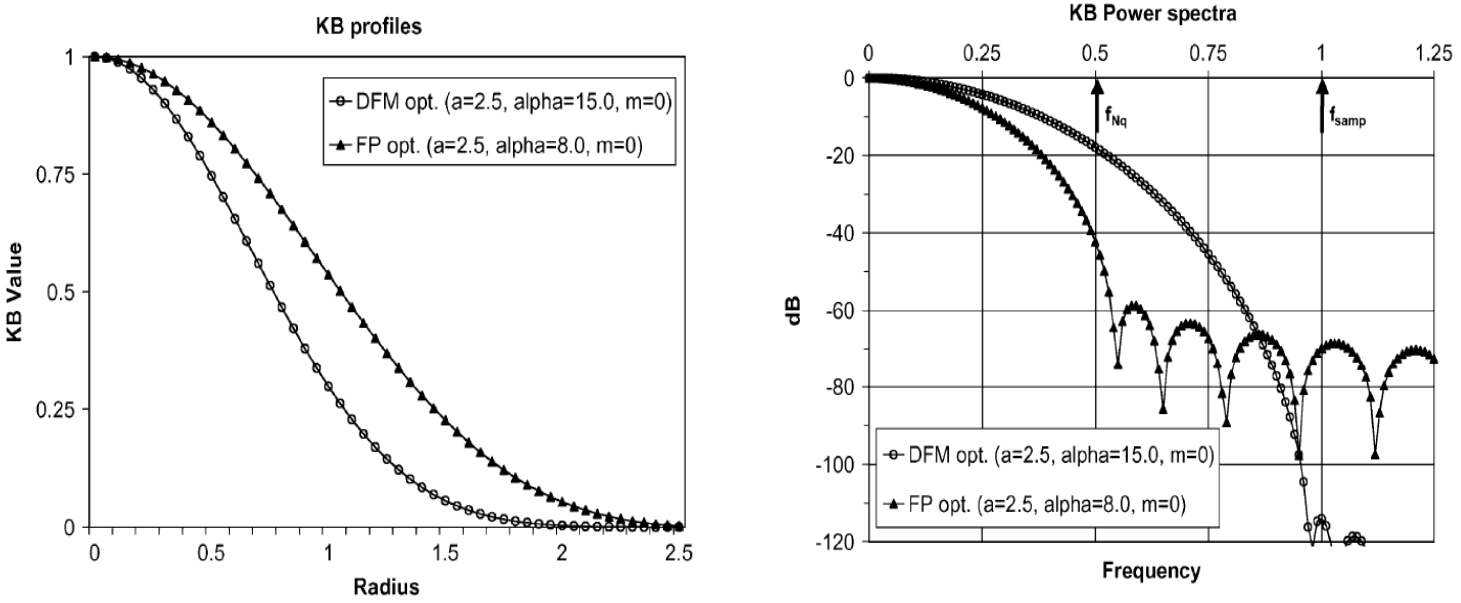

FIGURE 1 (a) The time-domain response of the MKB interpolation kernel for forward projection (FP) and the direct Fourier method (DFM). Parameters were optimized by looking for global minima in the normalize mean error of both procedures when compared to an ideal projection and real data respectively. (b) The corresponding Bode plot (amplitude of the 1D DFT of the Kernel). After Matej and Kazentsev, 2006.

The parameters a and m are optimized by the resolution of the reconstruction. In contrast to forward projection, the reprojection error is highly robust to z. In general, both errors are above the level introduced by quantization variance (and thus they can be optimized), but the minimum reprojection error using a 2D non-uniform Fast Fourier Transform (NUFFT) is several orders of magnitude lower than the reprojection error for the 3D interpolator. The reconstruction error for this interpolator is shown in FIGURE 3(a). This is probably due to the noise caused by reprojecting an estimated image. Furthermore, the parameter values used are different ($\alpha = 12$ for forward-projection and $\alpha = 16$ for reconstruction). This disparity is explained, firstly, by the fact that the data spectrum is homogenized by the pre-interpolation weighting function. Secondly, the even if the weighting function is not applied, we naturally expect the interpolator s to have different parameters because the spectrum has been expanded by the estimated values. In an actual PET experiment, the real parameters are expected to be different than the dry-optimized parameters. Thus, in order to optimize the parameters *de novo*, it would be necessary

to do FRP on only a small, but sufficient, subset of the data (preferably in areas of high variation in signal intensity).

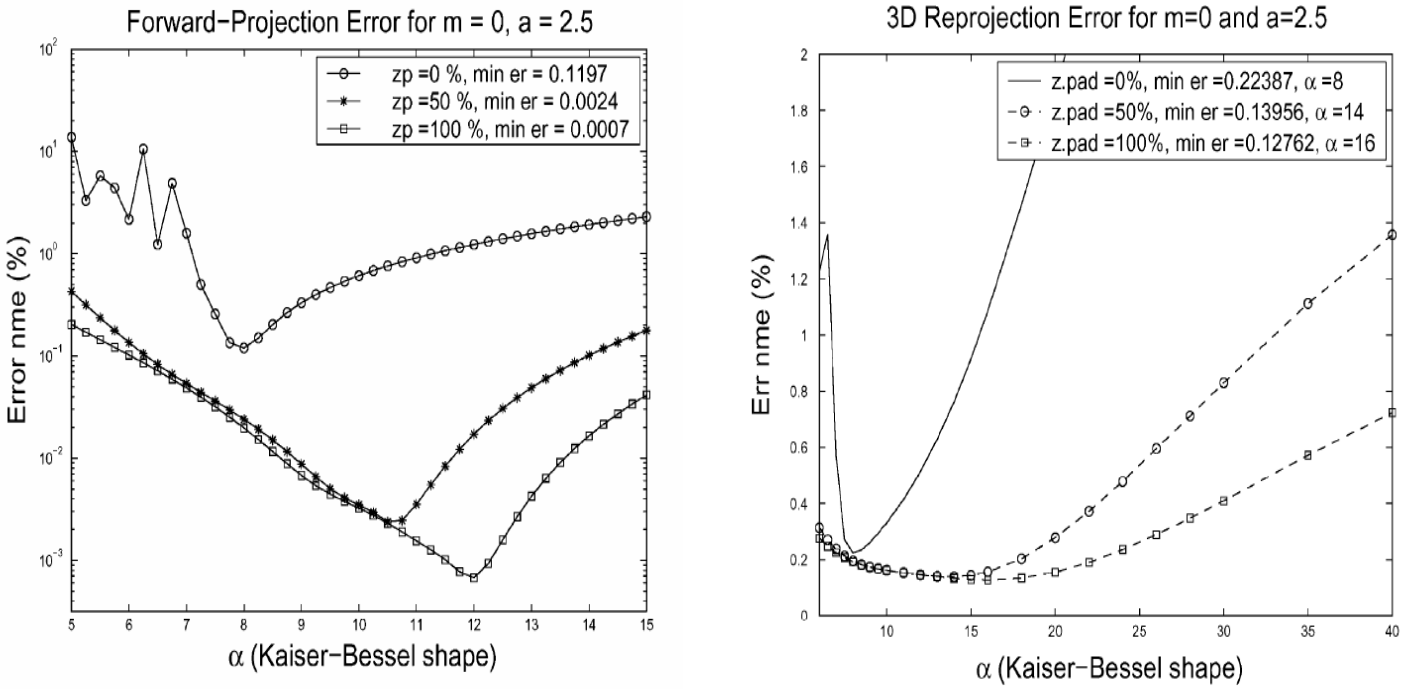

FIGURE 2 (a) Quantitative difference from an ideal projection (with a sinc interpolator) using the MKB kernel. (b) Differences for the reprojection step. After Matej and Kazentsev, 2006.

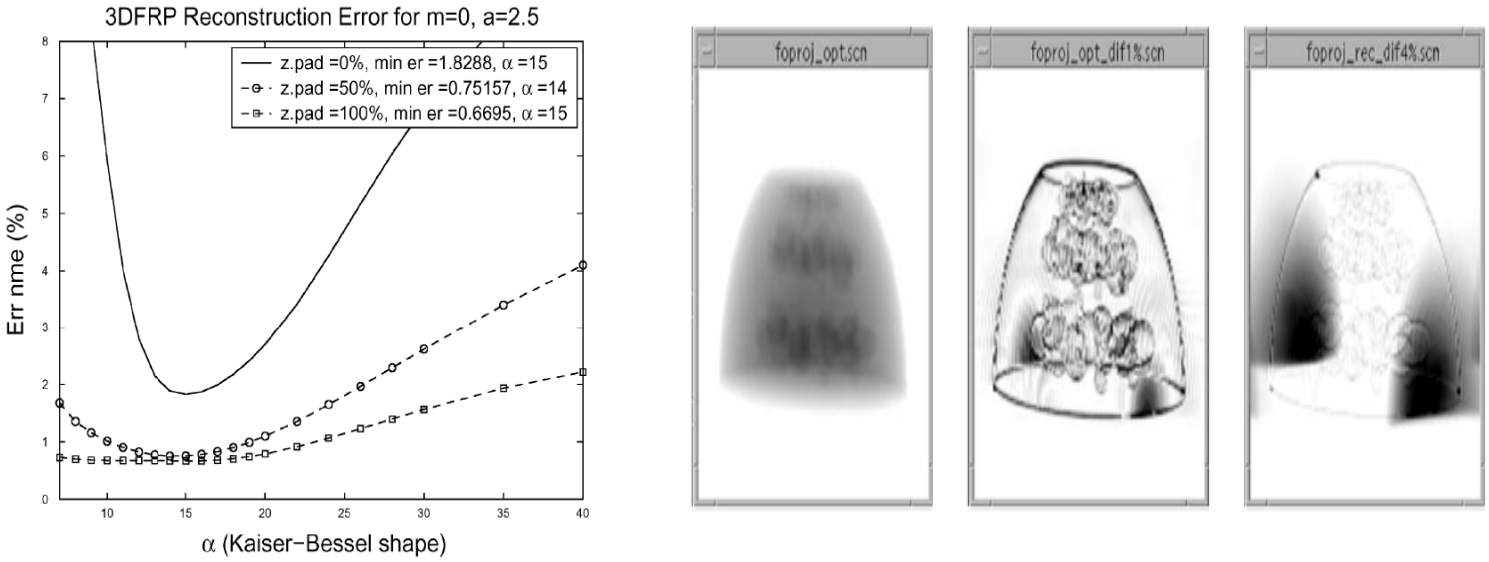

FIGURE 3 (a) The complete reconstruction error for a tissue phantom for optimized parameters and various zero-padding lengths. (b) Reconstruction of the tissue phantom with optimal parameters for both forward projection and reconstruction. (c) Error relative to the analytic projection and reconstruction. (d) A reconstruction in which the forward projection parameters are not optimized. After Matej and Kazentsev, 2006.

The resolution of the system was determined by viewing small sites of high activity (the local maxima in the phantom) as point sources. Since the reconstructed data is in voxelized form, a Point Spread Function (PSF) could be found from the data values surrounding this point. These data are shown in TABLE 1, and are, as expected, commensurate with the optimal parameters. It is a surprising result that the resolution itself is an inadequate means to optimize the parameters, since the FHWM is nearly constant as α is varied across an order of magnitude. This suggests that the resolution is a function of the native data (i.e., the number of samples in the data). The values obtained are similar to those reported (Yuan, communication). In contrast, the noise is a function of α, and is minimize (i.e., the variance is minimized) when α is optimized and the data is oversampled with $z = 1$. Similarly, the bias was minimized as well when α was optimized. The bias also varied with the amount of zero-padding.

Resolution of 3D FRP as determined from an approximate point source of activity. The Full-Width Half Maximum (FHWM) does not vary over a large range of α, indicating that the quality of the interpolation does affect the resolution.

Parameters			FWHM			FWTM		
m	a	α	Rad	Tang	Ax	Rad	Tang	Ax
0	2.5	6	4.70	4.28	5.50	9.79	8.83	11.03
		8	4.70	4.27	5.50	9.80	8.83	11.02
		15	**4.70**	**4.26**	**5.49**	**9.80**	**8.84**	**11.03**
		30	4.70	4.29	5.51	9.78	9.10	11.09
	3.5	30	4.70	4.27	5.50	9.80	8.85	11.03
2	2.5	12	4.70	4.27	5.49	9.80	8.85	11.03

The computation time for 3D FRP was reduced TO approximately 2.6% of the time required for a comparable reconstruction using standard iterative techniques (21s and 817s respectively), and was found to be dependent on the amount of zero padding. The data could be zero-padded at its full length ($z = 1$) with only an increase by 1.69 of the non-padded projections. (Matej and Kazantsev, 2006).

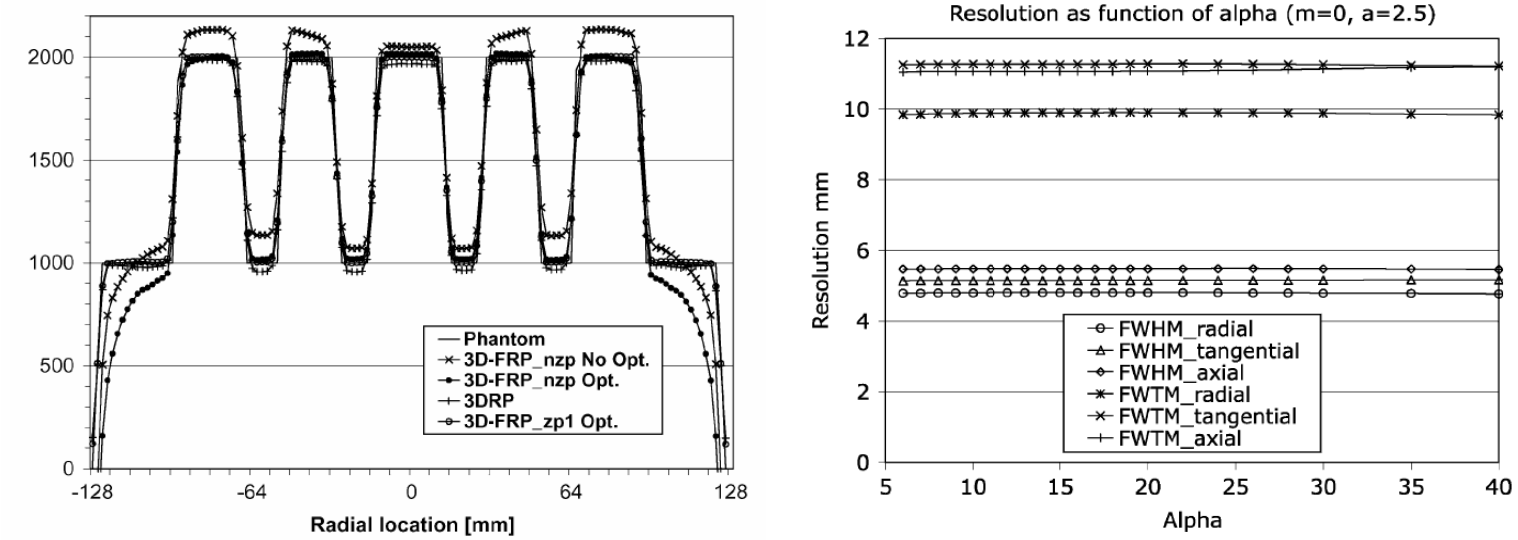

FIGURE 4 (a) Profiles of the tissue phantom (with a series of highly active foci) after reconstruction for various parameters. (b) Resolution of the direct Fourier method (Full Width Half Maximum) along three axes. After Matej and Kazentsev, 2006.

6 Refinements of the Direct-Fourier Algorithm

The optimization, thus far, has been based on the difference between the direct Fourier estimation and ideal (analytic) solutions. We suppose an equivalent result could be obtained if the parameters, collected as $(\alpha, a, m)^*$, were chosen such that the finite-kernel interpolation effect approaches the sinc effect. This could be done with a simply minimization algorithm:

$$(\alpha, a, m)^* = (\alpha, a, m) \,|\, \min\left\{ \left\langle \Im^{(2)} \langle p(r,\theta) \rangle \cdot \kappa(\bar{r}, \bar{\theta},) \cdot k(\omega) \right\rangle - \left\langle \Im^{(2)} \langle p(r,\theta) \rangle \cdot \frac{s(\bar{r}, \bar{\theta})}{k(\omega)} \cdot \Im \left\langle \frac{\sin \tau\theta}{\tau\theta} \right\rangle \right\rangle \right\} \quad (8)$$

This method only returns parameters that are unique to the data set (i.e., the projections). To translate this algorithm to clinical use,

The authors have only optimized the parameters for the MKB kernel. A similar process can be carried out for other filters. Indeed, any Finite Impulse Response filter could be optimized using the minimization algorithm.

Since the MKB window is time-symmetric, there is a well-defined group delay which can be determined from the transfer-function of the interpolator. This is simply given by $k(\omega)$. Thus, the group delay is given by the expression from (4):

$$\frac{\partial \phi}{\partial \omega} = \tan^{-1}\left(\mathrm{Re}\left\langle \left[\sqrt{1-(\omega/a)}\right]^m \cdot J\left(\alpha\sqrt{1-(\omega/a)}, m\right) \right\rangle \Big/ \mathrm{Im}\left\langle \left[\sqrt{1-(\omega/a)}\right]^m \cdot J\left(\alpha\sqrt{1-(\omega/a)}, m\right) \right\rangle \right) \cdots \\ \cdots - \tan^{-1}\left(\mathrm{Re}\, J(\alpha, m) / \mathrm{Im}\, J(\alpha, m)\right) \quad (9)$$

We have used the explicit formulation of the modified Bessel function below. The expression yields a constant (since the parameters are constant), which is equivalent to the standard form of the group delay. This is a linear function of the tap (i.e., length in the time domain) and the sampling frequency. The phase response above can be minimized as a function of the three parameters (used to optimize the error).

$$\frac{\partial \phi}{\partial \omega} = \tan^{-1}\left(\mathrm{Re}\left\langle \sum_{j=1}^{\infty} \left(\frac{(-1)^j}{j!\Gamma(j+m+1)} \cdot \left(\frac{1}{2} \cdot \alpha\sqrt{1-(\omega/a)} \right)^{2j} \right) \right\rangle \Big/ \mathrm{Im}\left\langle \sum_{j=1}^{\infty} \left(\frac{(-1)^j}{j!\Gamma(j+m+1)} \cdot \left(\frac{1}{2} \cdot \alpha\sqrt{1-(\omega/a)} \right)^{2j} \right) \right\rangle \right) \cdots \\ \cdots - \tan^{-1}\left(\mathrm{Re}\left\langle \sum_{j=1}^{\infty} \left(\frac{(-1)^j}{j!\Gamma(j+m+1)} \cdot \left(\frac{\alpha}{2} \right)^{2j} \right) \right\rangle - \mathrm{Im}\left\langle \sum_{j=1}^{\infty} \left(\frac{(-1)^j}{j!\Gamma(j+m+1)} \cdot \left(\frac{\alpha}{2} \right)^{2j} \right) \right\rangle \right) \quad (10)$$

The FRP algorithm can be used jointly with FORE in a scheme in which the rebinned projections are used to optimize the parameters. Similar approaches could be implemented with the iterative algorithms.

9 References

1. Matej and Kazantsev. Fourier-Based Reconstruction for Fully 3-D PET: Optimization of Interpolation Parameters. IEEE TRANSACTIONS ON MEDICAL IMAGING, VOL. 25, NO. 7, JULY 2006.

2. Kinahan et al. A Comparison of Transform and Iterative Reconstruction Techniques for a Volume-Imaging PET Scanner with a Large Axial Acceptance Angle. IEEE TRANSACTIONS ON NUCLEAR SCIENCE, VOL. 42, NO. *6*, DECEMBER 1995.

3. Bailey et al. An Investigation of Factors Affecting Detector and Geometric Correction in Normalization of 3-D PET Data. IEEE TRANSACTIONS ON NUCLEAR SCIENCE, VOL. 43, NO. 6, DECEMBER 1996

4. Rajan et al. High-speed Computation of the EM Algorithm for PET Image Reconstruction. IEEE TRANSACTIONS ON NUCLEAR SCIENCE, VOL. 41, NO. *5*, OCTOBER 1994

5. Badawi et al. The Effect of Camera Geometry on Singles Flux, Scatter Fraction and Trues and Randoms Sensitivity for Cylindrical 3D PET - a Simulation Study. IEEE TRANSACI'IONS ON NUCLEAR SCIENCE, VOL 47, NO. 3, JUNE 2000

6. Liu et al. Comparison of 3-D Reconstruction With 3D-OSEM and With FORE+OSEM for PET. IEEE TRANSACTIONS ON MEDICAL IMAGING, VOL. 20, NO. 8, AUGUST 2001

7. Kudrolli and Wostell. SS3D—Fast Fully 3-D PET Iterative Reconstruction Using Stochastic Sampling. IEEE TRANSACTIONS ON NUCLEAR SCIENCE, VOL. 49, NO. 1, FEBRUARY 2002

8. Panin et al. Fully 3-D PET Reconstruction With System Matrix Derived From Point Source Measurements. IEEE TRANSACTIONS ON MEDICAL IMAGING, VOL. 25, NO. 7, JULY 2006

9. Kinahan et al. Numerical Observer Studies Comparing FORE + AWOSEM, FORE + NECOSEM and NEC Based Fully 3-D OSEM for 3-D Whole-Body PET Imaging. IEEE TRANSACTIONS ON NUCLEAR SCIENCE, VOL. 53, NO. 3, JUNE 2006